R-MATRIX CALCULATION OF SINGLY IONIZED CARBON STRUCTURE FOR X-RAY LASER MODELLING

C. IORGA, V. PĂIŞ, V. STĂNCĂLIE

Department of Lasers, INFLPR, RO-077125, POB-MG36, Măgurele-Bucharest, Romania
E-mail: iorga.cristian@inflpr.ro, viorica.stancalie@inflpr.ro

Received July 4, 2015

This study presents the results of extensive calculations for the singly ionized carbon ion based on the electron scattering on the C^{2+} ion in the frameworks of the R-matrix theory. Combining the R-matrix and Quantum defect theory and method the Rydberg series of resonances have been identified. Comparison with other data has been made.

Part of present calculation results includes the oscillator strengths, collision strengths and photoionization cross sections which are further used to benchmark the data needed to perform the population kinetics in plasma.

The laser-produced carbon plasma is investigated for X-ray emission. Competing processes describing the level population distribution include autoionization, Auger decay and collisional ionization of the outer-shell electrons by electrons generated during the photoionization.

Key words: Carbon plasma, atomic structure, atomic and ionic spectroscopy, R-matrix method.

1. INTRODUCTION

A great and compact source for brilliant X-ray emission is represented by the laser-produced plasma [1]. The K-shell and L-shell transitions from carbon plasma have been intensively studied throughout the last decades [2–5]. Singly ionized carbon transitions in astrophysical plasmas have been investigated while including the effect for the X-ray presence on the ionization balance [6]. Further studies and modelling are necessary to improve the theoretical results.

The goal of this paper is to complete with additional information on atomic structure for the singly ionized carbon ion and level population kinetics calculations in high intensity laser-produced plasma environment for further use in X-ray laser modeling. The close-coupling R-matrix method and code [7] is well known and has been intensively used for calculating accurate data throughout the last decades [7–9]. The Breit-Pauli R-matrix method (BPRM) considers the semi-relativistic contributions of the mass, Darwin and spin-orbit terms while working with configurations in the intermediate coupling scheme thus becoming suitable for accurately calculating fine structure terms. It is stated that the fine structure levels in a plasma subjected to external or self-produced X-ray radiation are not identically populated [10], thus requiring high accuracy calculation.

The paper is structured as follows. The second section presents the R-matrix method of calculation, the Breit-Pauli approximation and the treatment for the collisional impact excitation and photoionization processes for C^+. The third section is concerned with population kinetics in laser-produced carbon plasma showing results from collisional radiative model calculations. Section four gives the concluding remarks.

2. R-MATRIX METHOD AND CALCULATIONS

The first step in employing the R-matrix method is to partition the configuration space into distinct regions by a sphere of radius a having its center in the nucleus, namely the internal region $(r \leq a)$ where exchange and correlation effects between the target and the scattered electron have to be considered and the external region $(r > a)$ where these effects are neglected and the outer electron moves in the potential created by the target.

Initially, there are N electrons inside the internal region forming a bound complex. This system is written as a configuration-interaction (CI) expansion in terms of some basis configurations that are constructed from a bound orbital basis consisting of self-consistent field orbitals along with pseudo-orbitals to account for electron correlation effects. The $(N+1)th$ electron is added to the internal region. The exchange and correlation effects between the previous N electrons and the "scattered" electron have to be taken into account, since they are considered to be indistinguishable particles. This $(N+1)$ electron system is now treated like a bound complex. The corresponding non-relativistic Hamiltonian of the system is given by:

$$H_{NR}^{N+1} = \sum_{n=1}^{N+1}(-\frac{1}{2}\nabla_n^2 - \frac{Z}{r_n} + \sum_{m>n}^{N+1}\frac{1}{r_{nm}}) \tag{1}$$

where the terms represent the kinetic, potential and self-interaction contributions.

In the Breit-Pauli R-matrix (BPRM) theory the Hamiltonian is given as follows:

$$H_{BP}^{N+1} = H_{NR}^{N+1} + H_{Mass}^{N+1} + H_{Darwin}^{N+1} + H_{SO}^{N+1} \tag{2}$$

where H_{NR}^{N+1} is the non-relativistic Hamiltonian, H_{Mass}^{N+1} is the one-body mass-velocity term, H_{Darwin}^{N+1} is the Darwin term and H_{SO}^{N+1} is the spin-orbit term. Relativistic fine-structure transitions in the Breit-Pauli approximation may be considered with an intermediate JK pair-coupling representation:

$$\begin{aligned} \vec{J}_{target} + \vec{l}_{e^-} &= \vec{K} \\ \vec{K} + \vec{s}_{e^-} &= \vec{J} \end{aligned} \tag{3}$$

where $\vec{l}_{e^-}$ and $\vec{s}_{e^-}$ are the orbital and spin angular momentum of the free electron, respectively. The total angular momentum $\vec{J}_{target}$ refers to the target level.

In the present paper the C^+ structure is calculated through the electron scattering of the C^{2+} ion. The target consists of 26 terms which include the 6 terms of Berrington *et al.* [11], namely $2s^2(^1S^e), 2s2p(^3P^o), (^1P^o)$ and $2p^2(^3P^e), (^1D^e), (^1S^e)$, plus all terms of the configurations $2s\bar{3}l$ and $2p\bar{3}l$ with $l = 0,\ 1,\ 2$. Using the above mentioned 26 term target extensive calculation has been carried out using the R-matrix code in intermediate coupling scheme.

The coupled-channel wave function in the inner region for the $C^{2+} + e^-$ system at a given symmetry $J\pi$ (in an intermediate coupling scheme) is expressed as products of the target ion states and partial waves (for the colliding electron)

$$\psi(E, e^- + C^{2+}) = \sum_i \chi_i(C^{2+})\theta_i(l_{e^-}) + \sum_j c_j\phi_j(C^{1+}) \tag{4}$$

Here, ψ denotes the continuum $(E > 0)$ states of a given symmetry $J\pi$, expanded in terms of the core ion eigenfunctions, $\chi_i(C^{2+})$ with a specific total angular momentum and parity conservation $J_l\pi_l$, and the l_{e^-} partial wave $\theta_i(l_{e^-})$ for the colliding $(N+1)$th electron with wave number k_{e^-} in a channel labeled $J_l\pi_l k_{e^-} l_{e^-}[J\pi]$ (the channel being either closed, $k_i^2 < 0$, or open, $k_i^2 \geq 0$, depending on the sign of its energy). The correlation wavefunctions $\phi_j(C^{1+})$ are introduced in the expansion for the $(N+1)$ bound electron system to compensate for the orthogonality conditions imposed on continuum with bound orbitals and to represent additional short-range correlations, which are important in scattering and radiative close coupling calculations.

For different combinations of angular momenta and parity, $SL\pi$, in the case of $e^- + C^{2+}$ system, the C^+ bound states form Rydberg series converging to the lowest C^{2+} states included in the close-coupling expansion. The energies E_n are expressed in terms of quantum defects ν_n defined as:

$$E_n = E_\infty - \frac{z^2}{\nu^2} \tag{5}$$

with $z = 2$ for C^+.

The program reads the data produced by STG3 and, for each $SL\pi$, calculates the positions of all bound states with ν_n in the range $\nu_{min} < \nu_n < \nu_{max}$.

The series $SL\pi = {}^2S,\ {}^2P^o,\ {}^2D,\ {}^2F^o,\ {}^2G$ and ${}^2H^o$ give levels converging to the C^{2+} ground state, $2s^2\ {}^1S$ other values of $SL\pi$ give levels converging to excited states of C^{2+}. Considering the series converging to $2s^2\ {}^1S$, the quantum defects may be plotted against an energy variable ϵ, defined by:

$$E = E_1 + z^2\epsilon_1 \tag{6}$$

where $E_1 = E(2s^2\ {}^1S)$. For the bound states $\epsilon_1 = -\frac{1}{\nu^2}$ and the quantum defect μ_n is

Table 1

The $J = 1/2,\ \pi = even$ symmetry effective quantum numbers obtained in this work along with the experimental values from http://www.nist.gov/pml/data/asd.cfm [12] and the ones calculated theoretically [8].

Term configuration	$\nu_{present}$	ν_{exp}	ν_{theory}
$2s2p^2(^4P_{1/2})$	1.68	1.69	
$2s2p^2(^2S_{1/2})$	2.11	2.09	
$2s2p^2(^2P_{1/2})$	2.27	2.26	
$2s^23s(^2S_{1/2})$	2.34	2.34	2.30
$2s^24s(^2S_{1/2})$	3.34	3.34	3.34
$2s^25s(^2S_{1/2})$	4.34	4.34	4.43
$2s^26s(^2S_{1/2})$	5.34	5.34	5.43
$2s2p(^3P^o)3p(^4D_{1/2})$	5.41	5.41	
$2s2p(^3P^o)3p(^2P_{1/2})$	5.48	5.47	
$2s^27s(^2S_{1/2})$	6.34	6.33	6.34
$2s2p(^3P^o)3p(^4P_{1/2})$	6.59	6.56	
$2s^28s(^2S_{1/2})$	7.34		7.34
$2s^29s(^2S_{1/2})$	8.33		8.33
$2s^210s(^2S_{1/2})$	9.32		9.33

Table 2

The $J = 3/2,\ \pi = even$ symmetry effective quantum numbers obtained in this work along with the experimental values from http://www.nist.gov/pml/data/asd.cfm [12] and the ones calculated theoretically [8].

Term configuration	$\nu_{present}$	ν_{exp}	ν_{theory}
$2s2p^2(^4P_{3/2})$	1.68	1.69	
$2s2p^2(^2D_{3/2})$	1.90	1.90	
$2s2p^2(^2P_{3/2})$	2.27	2.26	
$2s^23d(^2D_{3/2})$	2.93	2.93	2.91
$2s^24d(^2D_{3/2})$	3.92	3.92	3.92
$2s^25d(^2D_{3/2})$	4.91	4.91	4.92
$2s2p(^3P^o)3p(^4D_{3/2})$	5.41	5.42	
$2s2p(^3P^o)3p(^2P_{3/2})$	5.49	5.48	
$2s^26d(^2D_{3/2})$	5.90	5.90	5.91
$2s2p(^3P^o)3p(^4S_{3/2})$	6.07	6.05	
$2s2p(^3P^o)3p(^4P_{3/2})$	6.57	6.55	
$2s^27d(^2D_{3/2})$	6.87	6.86	6.88
$2s2p(^3P^o)3p(^2D_{3/2})$	7.46	7.36	
$2s^28d(^2D_{3/2})$	7.99		8.05
$2s^29d(^2D_{3/2})$	8.95		8.96
$2s^210d(^2D_{3/2})$	9.94		9.95

defined by $\nu_n = n - \mu$, where n is chosen to be such that $0 \leq \mu_n \leq 1$. Above $2s^2\ ^1S$ limit $\epsilon_1 > 0$ and μ is defined as $\mu = \frac{\delta}{\pi}$ where δ is the scattered phaseshift. Rapid variation of μ as a function of ϵ_1 corresponds to series perturbation for $\epsilon_1 < 0$ and to autoionization for $\epsilon_1 > 0$.

Table 3

The $J = 5/2$, $\pi = even$ symmetry effective quantum numbers obtained in this work along with the experimental values from http://www.nist.gov/pml/data/asd.cfm [12] and the ones calculated theoretically [8].

Term configuration	$\nu_{present}$	ν_{exp}	ν_{theory}
$2s2p^2(^4P)$	1.69	1.69	
$2s2p^2(^2D)$	1.90	1.90	
$2s^23d(^2D)$	2.93	2.93	2.91
$2s^24d(^2D)$	3.92	3.92	3.92
$2s^25d(^2D)$	4.91	4.91	4.92
$2s2p(^3P^o)3p^{\ 4}D$	5.41	5.42	
$2s^26d(^2D)$	5.90	5.90	5.91
$2s2p(^3P^o)3p(^4P)$	6.60	6.56	
$2s^27d(^2D)$	6.87	6.90	6.88
$2s2p(^3P^o)3p(^2D)$	7.47	7.38	
$2s^28d(^2D)$	7.99		8.05
$2s^29d(^2D)$	8.95		8.97
$2s^210d(^2D)$	9.94		9.95

The reactance matrix $\hat{K}$ is calculated from matching the solutions from the two regions at $r = a$. The scattering $\hat{S}$ and transmission $\hat{T}$ matrices are defined as:

$$\begin{aligned} \hat{S} &= (\hat{1} - i\hat{K})^{-1}(\hat{1} + i\hat{K}) \\ \hat{T} &= \hat{S} - \hat{1} \end{aligned} \tag{7}$$

The collision strength for transition from an initial state "i" to a final state "j" is given as:

$$\Omega_{ij} = \sum_{LS\pi} (\frac{g}{2} \sum_{l_i l_j} |T_{ij}|^2)^{LS\pi} \tag{8}$$

where the first summation is over all possible $LS\pi$ symmetries and the second summation is over the channels coupled to the initial and final states. The collision strength is plotted as a function of collision energy of the incoming electron in Fig.1.

To perform photoionization within the R-matrix framework, one needs to consider the situation when all the channels are closed in order to form the finite number of bound states from the $N + 1$ electron complex.

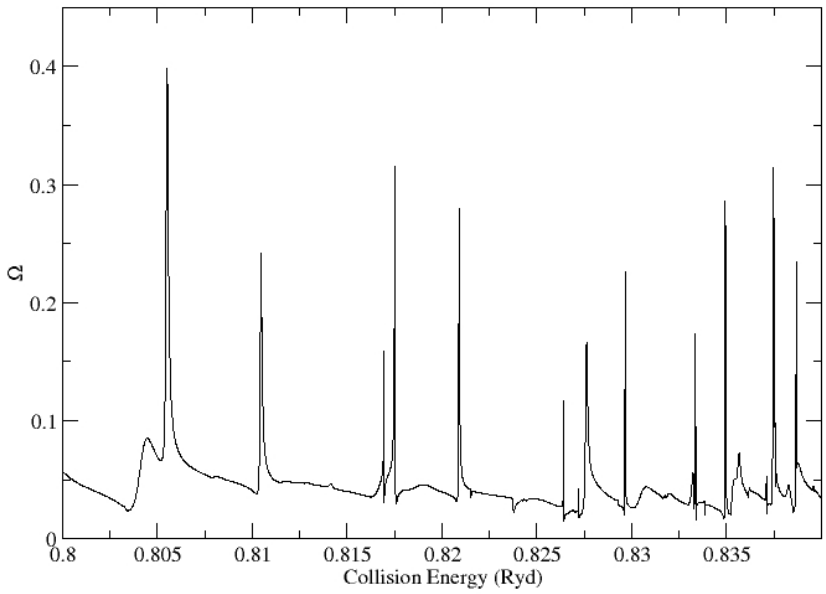

Fig. 1 – The collision strength is plotted against the electron energy.

The next step is to relate a certain bound state to all the continuum states of a given $J\pi$ symmetry through the dipole interaction. The corresponding dipole matrices calculated in length and velocity gauges give the line strength of the transition:

$$\begin{aligned} S^{(L)}(E_f;i) &= \sum_{Ll_f} \left| (Ll_f E_f \,||\, D^{(L)} \,||\, i) \right|^2 \\ S^{(V)}(E_f;i) &= \frac{4}{\omega^2} \sum_{Ll_f} \left| (Ll_f E_f \,||\, D^{(V)} \,||\, i) \right|^2 \end{aligned} \tag{9}$$

This leads to the photoionization cross section:

$$\sigma_{PI}^{(L,V)} = \frac{4}{3}\pi^2 a_0^2 \alpha \frac{\omega}{g} S^{(L,V)} \tag{10}$$

where a_0 is the Bohr radius, ω is the photon energy, α is the fine structure constant and g is the statistical weight.

This study reveals low lying, situated below the $C^{2+}1s^2 2s^2(^1S)$ threshold,

quartet configuration states belonging to the C^+. Figure 2 and Figure 3 present the total photoionization cross sections as output from the code. The graphs refer to the photoionization of C^+ from $1s^2 2s 2p^2(^3P)$ and $1s^2 2s 2p(^3P^o)3p(^4D, {}^4S, {}^4P)$ states to all C^{2+} states.

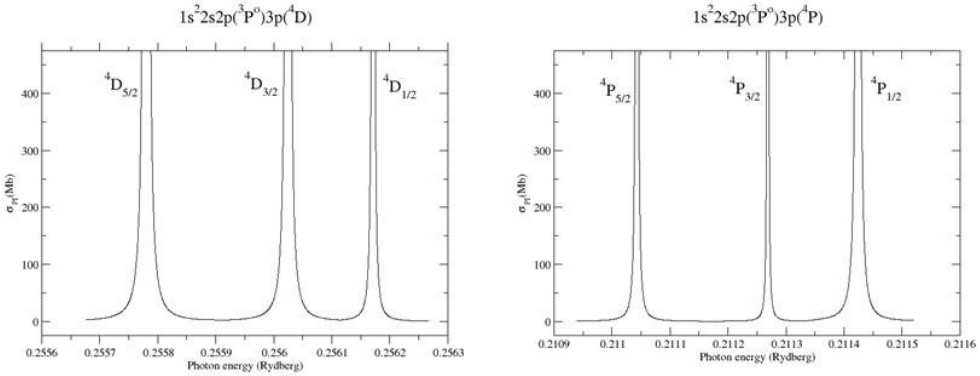

Fig. 2 – Photoionization of C^+ from the quartet configurations: $1s^2 2s 2p(^3P^o)3p\ (^4D),\ (^4P)$.

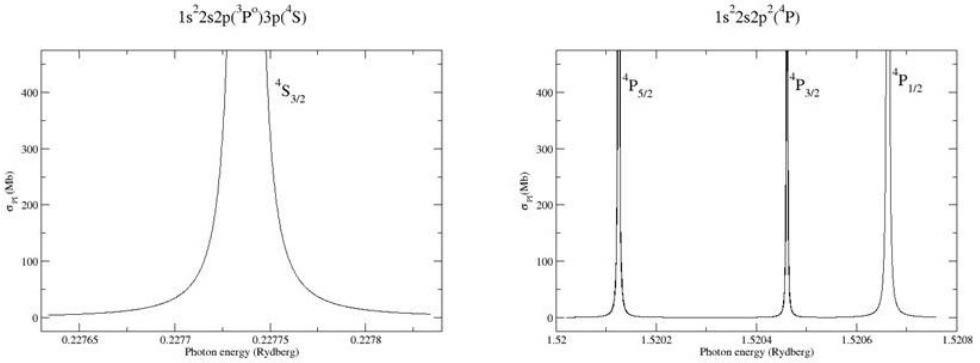

Fig. 3 – Photoionization of C^+ from the quartet configurations: $1s^2 2s 2p^2(^3P)$, $1s^2 2s 2p(^3P^o)3p(^4S)$.

3. PLASMA MODELLING

Laser-produced carbon plasma experiments resulting in high-line intensity transitions belonging to the C^+ ion have been performed [13, 14] using a Nd:YAG laser of 1.06μm. The goal of the present calculations is to give a set of optimal parameters for obtaining reasonably high X-ray emission sources. For this purpose the coupled equations for the level populations are solved within the collisional-radiative

model (CRM) assuming local thermodynamic equilibrium (LTE) and plasma quasi-neutrality condition:

$$\begin{aligned} &\frac{d\vec{n}}{dt} = \hat{R}\vec{n} \\ &\frac{N_{C^{(i+1)+}}}{N_{C^{i+}}} = \frac{g_{C^{(i+1)+}}}{g_{C^{i+}}} S e^{-\frac{E_{C^{i+}}}{k_B T}} \\ &\sum_i i \times N_{C^{i+}} = n_e \end{aligned} \tag{11}$$

where $\vec{n}$ is the vector containing the population for each energy level in the plasma, $\hat{R}$ is the matrix containing the rate coefficients for the relevant processes included in the model, $N_{C^{i+}}$ is the density for the C^{i+} ion, $g_{C^{i+}}$ is the weight function for the same ion, S is a parameter used in Saha equation and n_e is the electron density.

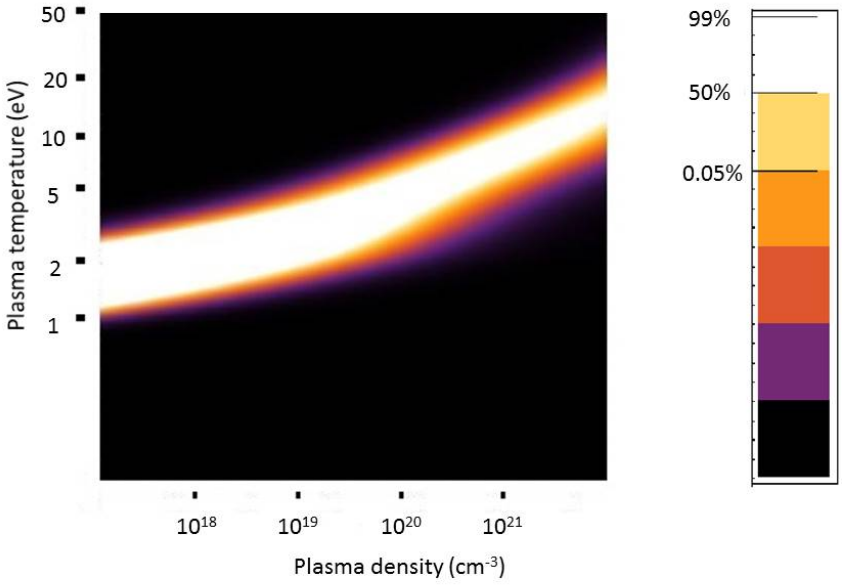

Fig. 4 – The ratio between the density of C^+ ion and the total ion density for relevant plasma temperature and electron density parameters.

Following the assumptions made earlier, a simulation has been performed for the density calculations for all degrees of ionization in a carbon plasma revealing the optimum parameters for having a dominating C^+ ion component. This is shown

in Fig.4 where the ratio between the C^+ density and the total ion density is plotted *versus* the plasma temperature and electron density. These parameters are obtainable in a laser-produced plasma experiment [13].

The CRM module of Flexible Atomic Code (FAC) [15] is well suited for optically thin plasmas in steady-state conditions. The processes treated in this model are: excitation, deexcitation, photoionization, radiative recombination, electron impact ionization, autoionization, dielectronic recombination and spontaneous decay. The atomic data used in this model are provided by the Flexible Atomic Code. Comparison with previous R-matrix results led to choosing an appropriate fictitious mean configuration capable of generating accurate data. The implemented model includes all ionization stages of carbon containing a total of 1492 energy levels, from which 465 correspond to the C^+ ion alone because it is the most dominant.

Table 4

The relative X-ray emissivity ratio for plasma containing high percentages of C^+ ions.

Plasma temperature (eV)	1.4	2.1	3.4	4.6	7	12
Plasma density (cm^{-3})	10^{17}	10^{18}	10^{19}	10^{20}	10^{21}	10^{22}
Relative X-ray emissivity ratio	0.07%	2.99%	59.81%	85.51%	92.08%	91.49%

The emissivity has been computed for the synthetic spectrum obtained within the collisional-radiative model framework. The X-ray contribution to the total emission is presented in Table 4. For this calculation the soft X-ray spectrum corresponding to the C^+ has been considered in the 3.7 nm-4.96 nm interval.

4. CONCLUSIONS

The intermediate-coupling R-matrix method and code (RMATXI) have been used to compute the atomic structure of the C^+. The results consist of resonances below the $1s^22s^2(^1S_0)$ threshold, collision strengths, and photoionization cross sections. Comparison with other theoretical and experimental works has been provided showing an overall good agreement. The cross sections corresponding to photoionization from several quartet levels belonging to singly ionized carbon have been proven to be quite high, dominating compared with the values obtained for the rest of the states by a few orders of magnitude. The study also reveals the optimum parameters of the laser-produced plasma containing a significant percentage of singly ionized carbon ions for emission of soft X-rays.

Acknowledgements. This work is partially supported by the Institute of Atomic Physics under project No. F03. Financial support under the Romanian program STAR Project Number 33 is also acknowledged.

REFERENCES

1. S. Fujioka, H. Nishimura, H. Takabe, N. Yamamoto, K. Nishikara, *et al.*, in *The Sixth International Conference on Inertial Fusion Sciences and Applications, Journal of Physics: Conference Series 244*, p. 012001 (2010).
2. J. Filevich, J. Grava, M. Purvis, M. C. Marconi, J. J. Rocca, J. Nilsen, Laser and Particle Beams **25**, 47–51 (2007).
3. D. Petrini, E. P. Silva, Astron. Astrophys **317**, 262–264 (1997).
4. B. B. Dhal, H. C. Padhi, K. G. Prasad, P. N. Tandon, M. Polasik, J. Phys B: At. Mol. Opt. Phys. **31**, 1225 (1998).
5. U. Majewska, K. Slabkowska, M. Polasik, J. Braziewicz, D. Banas, T. Czyzewki, I. Fijal, M. Jaskola, A. Korman, S. Chojnacki, J. Phys B: At. Mol. Opt. Phys. **35**, 1941 (2002).
6. W. D. Langer, J. L. Pineda, *[C II] emission from galactic nuclei in the presence of X-rays* (Accepted 27 May 2015).
7. K. A. Berrington, W. B. Eissner, P. H. Norrington, Computer Physics Communications **92**, 290–420 (1995).
8. S. N. Nahar, Atomic Data and Nuclear Data Tables **80**, 205–234 (2002).
9. P. Shorer, Journal of Phys, B: At Mol. Phys. **13**, 2921 (1980).
10. D. Benredjem, J. Dubau, O. Guilbaud, A. Klisnick, C. Moller, High Energy Density Physics **3(3-4)**, 335–341 (2007).
11. K. A. Berrington, P. G. Burke, P. L. Dufton, A. E. Kingston, J. Phys. B: At. Mol. Phys. **10(8)**, 1465 (1977).
12. A. Kramida, Y. Ralchenko, J. Reader, NIST ASD Team (2014), [Online]. Available: http://www.nist.gov/pml/data/asd.cfm (2015, July 3).
13. S. S. Harilal, C. V. Bindhu, R. C. Isaac, V. P. N. Nampoori, C. P. G. Vallabhan, j. Appl. Phys **82**, 2140 (1997).
14. A. P. S. R. Prasad, R. K. Thareja, Phys. Rev. E **48(4)**, 2929–2933 (1993).
15. M. F. Gu, Can. J. Phys. **86(5)**, 675–689 (2008).